Semiclassical approach for nuclear Coulomb excitation

Zongheng Li [1,*] Tao Li,[1,*] and Xu Wang [1,2,†]

[1]*Graduate School, China Academy of Engineering Physics, Beijing 100193, China*
[2]*Southern Center for Nuclear-Science Theory, Institute of Modern Physics, Chinese Academy of Sciences,*
Huizhou, Guangdong 516000, China

Nuclear Coulomb excitation is often calculated using a semiclassical (SC) approach, where the projectile follows classical trajectories and excites the target nucleus through a time-dependent Coulomb interaction. While the validity of the SC approach has been well established for electric quadrupole ($E2$) transitions, its accuracy for higher-order multipole transitions remains insufficiently benchmarked. In this paper, we compare Coulomb excitation cross sections for higher-order multipole transitions calculated using the SC approach with those obtained through a quantum mechanical (QM) approach, where the projectile is described by wave functions. For $E2$ transitions, the excitation cross sections from both approaches are of the same order of magnitude, consistent with existing validations. However, for higher-order multipole transitions, the SC approach yields significantly higher cross sections, deviating possibly by orders of magnitude from the QM results. This discrepancy underscores the necessity of the QM approach for accurate calculations of the Coulomb excitation cross sections. The failure of the SC approach is explained through using the Wentzel-Kramers-Brillouin approximation.

I. INTRODUCTION

Coulomb excitation is a process of inelastic scattering where a charged particle transfers energy to a target nucleus via electromagnetic interaction [1–6]. Over the past few decades, Coulomb excitation has been a well-established method in nuclear physics for exploring nuclear structures, and much nuclear structural information has been gained through this method over the years [7–14]. Recently, the use of radioactive ion beams has revitalized Coulomb excitation [15–17], enabling the study of short-lived exotic nuclei far from the β stability line [18–20].

The theoretical framework for Coulomb excitation has been extensively developed [3,21–24]. Often, a semiclassical (SC) approach is considered adequate and convenient for Coulomb excitation calculations [22,23,25], while a quantum mechanical (QM) approach, which involves computing wave functions for multiple states, is more intricate [26]. In the SC approach, excitation is caused by the electromagnetic field of the incident particle moving along a classical trajectory, whereas in the QM approach, excitation arises from the exchange of a virtual photon between the projectile and the nucleus. The validity of the SC approach for electric quadrupole ($E2$) transitions has been established [21,22,27–30]: the difference between these two approaches is shown to be insignificant at least in the regime where the so-called Sommerfeld parameter $\eta \gg 1$ (shown later). However, benchmarking the SC approach for higher-order multipole transitions remains scarce. This article aims to address whether the SC approach remains accurate for higher-order multipole transitions.

Our results indicate that it does not. For high-velocity incident particles, the cross sections obtained by the SC approach can deviate significantly from those obtained by the QM approach, with discrepancies ranging from 1 to 3 orders of magnitude. Quantum effects are therefore crucial in higher-order multipole Coulomb excitations. We present a comprehensive analysis based on the Wentzel-Kramers-Brillouin (WKB) approximation to explain this deviation.

This paper is organized as follows. Section II briefly introduces the two approaches for calculating Coulomb excitation. Section III presents numerical results and discusses the validity of the SC approach under different conditions. A conclusion is given in Sec. IV. For clarity and simplicity, this paper focuses on electric excitations, and analogous conclusions can be made for magnetic excitations.

II. METHODS

The theory of nuclear Coulomb excitation is well established [3,21–24]. Here, we outline the key derivations and formulas to provide a general understanding of the results obtained.

A. Semiclassical approach

In the SC treatment of Coulomb excitation, the incident projectile moves along a Rutherford scattering trajectory and the target nucleus is excited during the collision. The differential cross section of nuclear excitation is given by

$$d\sigma^c = P d\sigma_R. \tag{1}$$

Here, P is the probability that the nucleus is excited in a collision in which the projectile is scattered into the solid angle $d\Omega$, and $d\sigma_R$ is the differential cross section of Rutherford scattering given by

$$d\sigma_R = \frac{1}{4}a_0^2 \sin^{-4}\left(\frac{\theta}{2}\right)d\Omega, \tag{2}$$

where θ is the scattering angle, and $a_0 = Z_1 Z_2 e^2/mv_i^2$ is half the distance of closest approach in a head-on collision. Z_1 and Z_2 are the charge numbers of the projectile and the target nucleus, e is elementary charge, and v_i and m are the initial velocity and the mass of the incident particle, respectively.

Averaging over initial states and summing over final states, the nuclear excitation probability P is given by

$$P = \frac{1}{2I_i + 1}\sum_{M_i M_f}|b_{if}|^2, \tag{3}$$

where b_{if} is the transition amplitude from initial nuclear state $|i\rangle = |I_i M_i\rangle$ to final state $|f\rangle = |I_f M_f\rangle$ with I_i (I_f) being the spin of the initial (final) nuclear state, and M_i (M_f) being the corresponding magnetic quantum number. The transition amplitude b_{if} can be obtained from first-order perturbation theory as

$$b_{if} = \frac{1}{i\hbar}\int_{-\infty}^{\infty}\langle I_f M_f|H_I(t)|I_i M_i\rangle e^{i\Delta E t/\hbar}dt, \tag{4}$$

where $H_I(t)$ is the Coulomb interaction Hamiltonian between the moving projectile and the nucleus, and ΔE is the nuclear excitation energy. For electric excitations, b_{if} has the following form after expanding $H_I(t)$ into multipole components:

$$b_{if} = \frac{4\pi Z_1 e}{i\hbar}\int_{-\infty}^{+\infty}\sum_{\lambda=1}^{\infty}\sum_{\mu=-\lambda}^{\lambda}\frac{1}{2\lambda+1}Y_{\lambda\mu}(\theta,\phi)\frac{1}{r^{\lambda+1}}$$
$$\times \langle I_i M_i|\mathcal{M}_{\lambda\mu}^E|I_f M_f\rangle e^{i\Delta E t/\hbar}dt. \tag{5}$$

In the above formula, $\mathcal{M}_{\lambda\mu}^E$ is the electric multipole moment of the nucleus, $Y_{\lambda\mu}$ is the spherical harmonic function, and $\mathbf{r} = \{r(t), \theta(t), \phi(t)\}$ is the time-dependent position of the projectile from the centroid of the nucleus.

The differential cross section for an $E\lambda$ transition can be given as

$$d\sigma_\lambda^c = \left(\frac{Z_1 e}{\hbar v_i}\right)^2 a_0^{-2\lambda+2}B(E\lambda)$$
$$\times \frac{4\pi^2}{(2\lambda+1)^3}\sum_\mu\left|Y_{\lambda\mu}\left(\frac{\pi}{2},0\right)\right|^2|I_{\lambda\mu}|^2\sin^{-4}\left(\frac{\theta}{2}\right)d\Omega, \tag{6}$$

where $B(E\lambda) = \sum_{M_f\mu}|\langle I_i M_i|\mathcal{M}(E\lambda,\mu)|I_f M_f\rangle|^2$ is the reduced nuclear transition probability, and we have introduced

$$I_{\lambda\mu}(\xi_0,\epsilon) = \int_{-\infty}^{+\infty}e^{i\xi_0(\epsilon\sinh w+w)}$$
$$\times \frac{(\cosh w + \epsilon + i\sqrt{\epsilon^2-1}\sinh w)^\mu}{(\epsilon\cosh w + 1)^{\lambda+\mu}}dw, \tag{7}$$

which is obtained from time integration along the Rutherford scattering trajectory. The dimensionless quantity ξ_0 and trajectory eccentricity ϵ are defined by

$$\xi_0 = \frac{a_0\Delta E}{\hbar v_i}, \quad \epsilon = \frac{1}{\sin(\theta/2)}. \tag{8}$$

Since the SC approach neglects the effect of the energy loss on the motion of the projectile, the final velocity of the projectile v_f is not included in the calculation. To improve the accuracy of the SC approach, the cross sections can be symmetrized by replacing a_0 and ξ_0 with symmetrized parameters a and ξ given by [7]

$$a = \frac{Z_1 Z_2 e^2}{mv_i v_f}, \quad \xi = \frac{Z_1 Z_2 e^2}{\hbar}\left(\frac{1}{v_f} - \frac{1}{v_i}\right). \tag{9}$$

The total nuclear excitation cross section of order $E\lambda$, obtained by integrating over all scattering angles, is given by

$$\sigma_\lambda^c = \left(\frac{Z_1 e}{\hbar v_i}\right)^2 a^{-2\lambda+2}B(E\lambda)$$
$$\times \frac{16\pi^3}{(2\lambda+1)^3}\sum_\mu\left|Y_{\lambda\mu}\left(\frac{\pi}{2},0\right)\right|^2$$
$$\times \int_0^\pi\left|I_{\lambda\mu}\left(\xi,\sin^{-1}\left(\frac{\theta}{2}\right)\right)\right|^2\frac{\cos\left(\frac{\theta}{2}\right)}{\sin^3\left(\frac{\theta}{2}\right)}d\theta. \tag{10}$$

B. Quantum mechanical approach

In the QM approach, the projectile is described by wave functions, contrasting with the Rutherford scattering trajectories used in the SC approach. The state of the entire system is expressed as the product of the nuclear state $|IM\rangle$, the projectile scattering state $|\mathbf{k}\rangle$, and the photon number state of the radiation field $|n\rangle$. The initial and final states can be expressed as follows:

$$|i\rangle = |I_i M_i\rangle \otimes |\mathbf{k}_i\rangle \otimes |0\rangle,$$
$$|f\rangle = |I_f M_f\rangle \otimes |\mathbf{k}_f\rangle \otimes |0\rangle. \tag{11}$$

The interaction Hamiltonian H_I is given by

$$H_I = -\frac{1}{c}\int(\mathbf{j}_p(\mathbf{r}) + \mathbf{j}_n(\mathbf{r}))\cdot\mathbf{A}(\mathbf{r})d\tau$$
$$+ \int\frac{\rho_n(\mathbf{r})\rho_p(\mathbf{r}')}{|\mathbf{r}-\mathbf{r}'|}d\tau d\tau', \tag{12}$$

where c is the speed of light, $\mathbf{A}$ is the vector potential of the radiation field, $\rho_{n,p}$ and $\mathbf{j}_{n,p}$ are the charge density and current density of the nucleus and the projectile, respectively. For electric multipole transitions, the matrix element of H_I can be written as

$$\langle f|H_I|i\rangle = \sum_{\lambda\mu}\frac{4\pi}{2\lambda+1}(-1)^\mu$$
$$\times \langle\mathbf{k}_f|\mathcal{N}_{\lambda\mu}^E|\mathbf{k}_i\rangle\langle I_f M_f|\mathcal{M}_{\lambda-\mu}^E|I_i M_i\rangle \tag{13}$$

with the notations

$$\mathcal{N}_{\lambda\mu}^E = \frac{i\kappa^\lambda}{c\lambda(2\lambda-1)!!} \int \mathbf{j}_p \cdot \nabla \times \mathbf{L}\big[h_\lambda^{(1)}(\kappa r)Y_{\lambda\mu}(\theta,\phi)\big]d\tau,$$

$$\mathcal{M}_{\lambda\mu}^E = \frac{(2\lambda+1)!!}{c(\lambda+1)\kappa^{\lambda+1}} \int \mathbf{j}_n \cdot \nabla \times \mathbf{L}[j_\lambda(\kappa r)Y_{\lambda\mu}(\theta,\phi)]d\tau. \tag{14}$$

Here, $\mathbf{L}$ is the angular momentum operator, $h_\lambda^{(1)}$ is the spherical Hankel function of the first kind, and j_λ is the spherical Bessel function. $\kappa = \Delta E/\hbar c$ is the wave number corresponding to the nuclear excitation energy.

For an $E\lambda$ transition, when the projectile velocities $v_{i,f} \ll c$, the differential cross section of nuclear excitation is given by

$$d\sigma_\lambda^q = \frac{m^2}{4\pi^2\hbar^4}\frac{v_f}{v_i}\frac{1}{2I_i+1}\sum_{M_iM_f}|\langle f|H_I|i\rangle|^2 d\Omega$$

$$= \left(\frac{Z_1 e}{\hbar v_i}\right)^2 B(E\lambda)\frac{4k_ik_f}{(2\lambda+1)^3}$$

$$\times \sum_\mu |\langle \mathbf{k}_f|r^{-\lambda-1}Y_{\lambda\mu}(\theta,\phi)|\mathbf{k}_i\rangle|^2 d\Omega, \tag{15}$$

where $k_{i,f} = mv_{i,f}/\hbar$ are the wave numbers of the incident particle and the ejected particle, respectively. The total excitation cross section obtained by integration over the solid angles is given by

$$\sigma_\lambda^q = \left(\frac{Z_1 e}{\hbar v_i}\right)^2 B(E\lambda)\frac{64\pi^2}{(2\lambda+1)^2}k_ik_f$$

$$\times \sum_{l_il_f}(2l_i+1)(2l_f+1)\begin{pmatrix} l_i & l_f & \lambda \\ 0 & 0 & 0 \end{pmatrix}^2 \big|M_{l_il_f}^{-\lambda-1}\big|^2, \tag{16}$$

where the radial matrix element M is defined by

$$M_{l_il_f}^{-\lambda-1} = \frac{1}{k_ik_f}\int_0^\infty R_{l_f}(k_f r)r^{-\lambda-1}R_{l_i}(k_i r)dr \tag{17}$$

with $R_l(kr)$ being the radial wave function of the projectile with orbital angular momentum l. In this paper these wave functions are calculated using the code RADIAL [31].

To quantify the disparities between the cross sections obtained from the SC approach and QM approach, we introduce the ratio

$$R_\lambda = \frac{\sigma_\lambda^q}{\sigma_\lambda^c}, \tag{18}$$

where σ_λ^c and σ_λ^q are the SC and QM cross sections from Eqs. (10) and (16), respectively.

III. RESULTS AND DISCUSSIONS

In this section, we provide numerical results of the ratio R_λ for different multipole transitions. In the study of Coulomb excitation, two parameters, η and ξ, are frequently employed. The Sommerfeld parameter η is related to the initial velocity
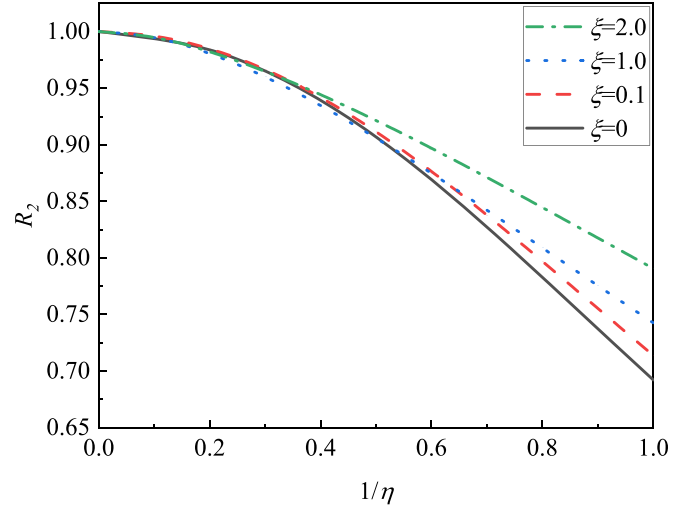

FIG. 1. The ratio R_2 for $E2$ transitions, plotted as a function of $1/\eta$ for $\xi = 0, 0.1, 1.0, 2.0$.

of the projectile

$$\eta = \frac{Z_1 Z_2 e^2}{\hbar v_i}, \tag{19}$$

and ξ has been defined in Eq. (9). A larger value of η corresponds to a lower incident velocity of the projectile, whereas a larger value of ξ represents more energy loss of the projectile due to Coulomb excitation.

A. SC vs. QM results for $E2$ transitions

Figure 1 shows the ratio R_2 for $E2$ transitions with ξ values of 0, 0.1, 1.0, and 2.0 and $1/\eta$ ranging from 0 to 1.0. One sees that the difference between σ_2^q and σ_2^c is not significant for $1/\eta < 1.0$, with the deviation reaching up to 30% when $\xi = 0$ and $1/\eta = 1.0$. This indicates that the accuracy of the SC approach is reliable in this range. Similar results are also seen for $E1$ transitions [3].

Additional insights include: (1) The ratio R_2 reaches its maximum value of 1.0 as $1/\eta \to 0$. This corresponds to the classical limit, where the initial velocity of the projectile is low and the distance from the nucleus is kept large due to the mutual Coulomb repulsion. (2) For the same value of $1/\eta$, R_2 increases with the value of ξ. It indicates that the discrepancy between σ_2^q and σ_2^c decreases as the excitation energy increases.

B. SC vs. QM results for higher-order multipole transitions

Figure 2(a) presents the ratio R_λ for $E2$, $E3$, $E4$, and $E5$ transitions with $\xi = 0$ and $1/\eta$ ranging from 0 to 2.0, demonstrating the significant influence of the order of multipole transitions. As the order λ increases, the ratio R_λ quickly decreases, indicating larger discrepancies between the SC cross sections and the QM results. The discrepancy can become as large as 1 to 3 orders of magnitude. The results are similar for $M2$, $M3$, $M4$, and $M5$ transitions as shown in Fig. 2(b).

As mentioned above, the benchmarking of the SC approach has been mostly confined to $E1$ and $E2$ transitions. As far as we are aware of, the SC approach has not been validated for
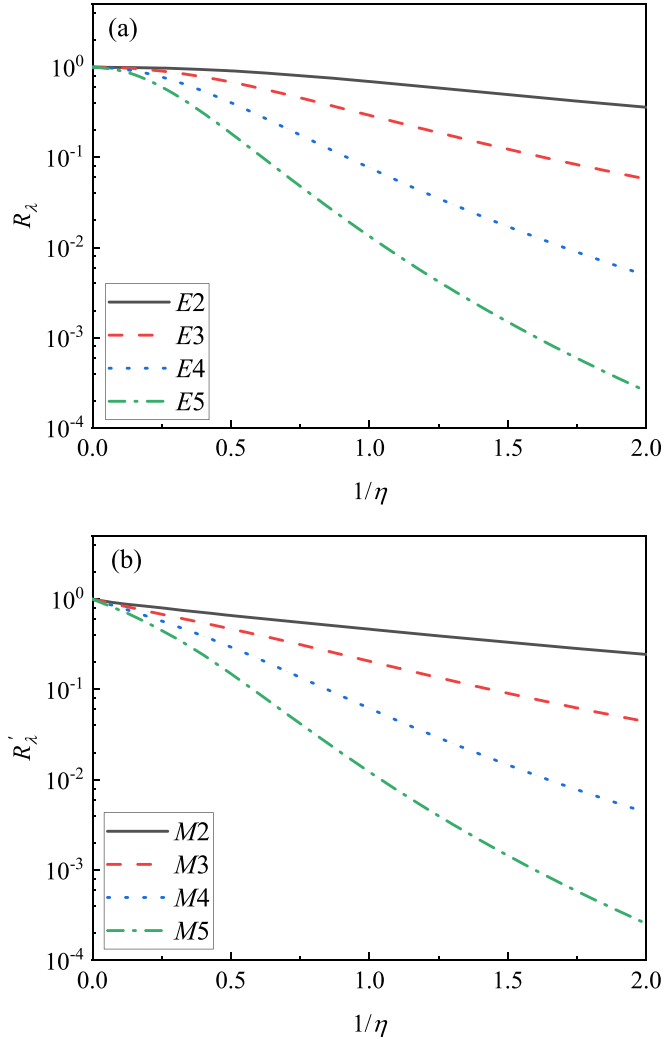
FIG. 2. (a) R_λ for electric multipole excitations with $\lambda = 2, 3, 4,$ 5, plotted as a function of $1/\eta$ for $\xi = 0$. (b) The ratio of magnetic multipole excitation cross sections obtained by the QM approach and those obtained by the SC approach, denoted by R'_λ. The ratio R'_λ is plotted as a function of $1/\eta$ for $\xi = 0$.

higher order multipole transitions. Furthermore, the collision parameter η is usually taken to be $\eta \gg 1.0$, a practice generally valid for heavy nucleus collisions. However, in the context of high-velocity projectile bombarding light nucleus, η tends to approach or even fall below 1.0. Hence, it is essential to take both of these scenarios into account.

C. Examples of comparison: ^{19}F and ^{83}Kr

To gain a clearer understanding of the differences between σ_λ^c and σ_λ^q, we calculate the excitation cross sections for protons bombarding ^{19}F and ^{83}Kr. ^{19}F has an $E2$ transition channel of $1/2^+ \rightarrow 5/2^+$ with an excitation energy of 197 keV, while ^{83}Kr has an $E5$ transition channel of $9/2^+ \rightarrow 1/2^-$ with an excitation energy of 41 keV. These two transitions have both attracted experimental interest [32,33]. The calculated excitation cross sections are shown in Fig. 3. For ^{19}F, we use the reduced transition probability from the
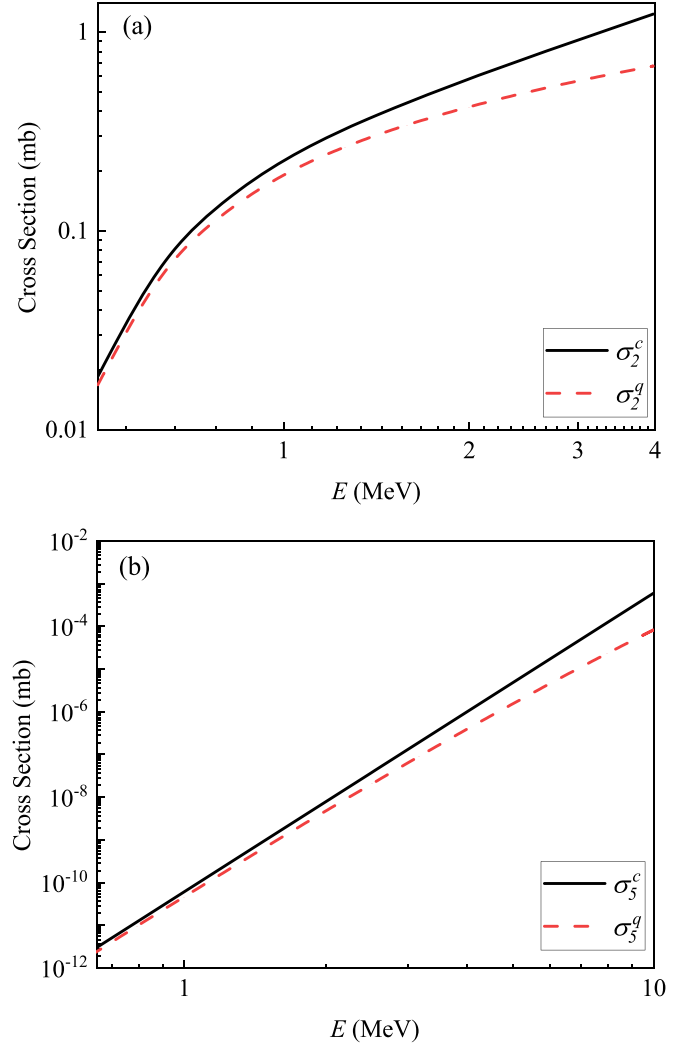

FIG. 3. (a) Nuclear excitation cross section of the 197 keV nuclear level of ^{19}F by protons, calculated by the SC approach (black solid curve) and by the QM approach (red dashed curve). (b) Nuclear excitation cross section of the 41 keV nuclear level of ^{83}Kr by protons calculated by the SC approach (black solid curve) and by the QM approach (red dashed curve).

National Nuclear Data Center (NNDC) with $B(E2, e \rightarrow g) = 6.95$ W.u. [34]. For ^{83}Kr, since the $E5$ excitation channel has not been experimentally measured, we use the Weisskopf approximation, estimating the reduced transition probability as $B(E5, e \rightarrow g) = 1$ W.u.

Figure 3(a) shows the comparison between the SC and the QM cross sections for ^{19}F. The discrepancy between σ_2^c and σ_2^q gradually increases with rising proton energy. At a proton energy of 4 MeV, corresponding to a collision parameter of $1/\eta = 1.4$, the SC cross section is about twice the value of the QM cross section.

Figure 3(b) displays the comparison for ^{83}Kr. Here, the discrepancy also grows with rising proton energy. At a proton energy of 10 MeV, corresponding to $1/\eta = 0.6$, the SC cross section is about an order of magnitude higher than the QM value. In both cases, the proton energies are sufficiently low, ensuring that the protons remain outside the target nuclei.
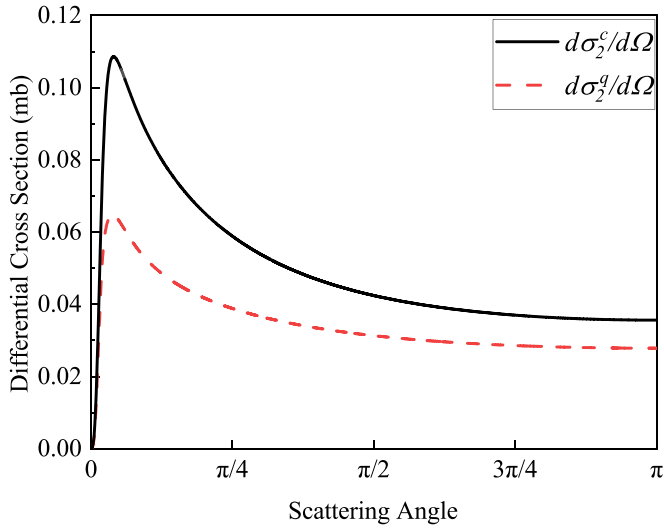
FIG. 4. Differential cross section of ^{19}F excited by 2 MeV protons, calculated by the SC approach (black solid curve) and by the QM approach (red dashed curve).

Additionally, Fig. 4 presents the differential excitation cross section of ^{19}F excited by protons with an energy of 2 MeV. The differential cross sections obtained through both approaches exhibit similar trends, except for a difference in overall amplitude.

D. The WKB approximation and the classical limit

The WKB approximation offers a convenient means of contrasting the disparities between SC approach and QM approach [22,35]. Using the WKB-approximated wave function for the projectile, the radial matrix element of Eq. (17) in the QM approach can be related to the orbital integral of Eq. (7) in the SC approach [28,36]:

$$M_{l_i,l_f}^{-\lambda-1} = \frac{k_0^{\lambda-2}}{4\eta_0^\lambda} I_{\lambda\mu_0}(\xi, \epsilon_0), \tag{20}$$

where $k_0 = (k_i + k_f)/2$ and $\eta_0 = ak_0$, and the parameters in the orbital integral are given by

$$\mu_0 = l_f - l_i,$$

$$\epsilon_0 = \frac{\sqrt{\eta_0^2 + (l_i + \mu_0/2)(l_i + 1 + \mu_0/2)}}{\eta_0}. \tag{21}$$

The WKB approximation is valid for $\eta_0 > 1$. Inserting Eq. (20) into Eq. (16), the WKB-approximated quantum excitation cross section can be written as

$$\sigma_\lambda^q = \left(\frac{Z_1 e}{\hbar v_i}\right)^2 a^{-2\lambda+2} B(E\lambda) \frac{k_i k_f}{k_0^2} \frac{16\pi^3}{(2\lambda+1)^3} \sum_\mu \left| Y_{\lambda\mu}\left(\frac{\pi}{2}, 0\right) \right|^2$$

$$\times \sum_{l_i} \frac{1}{\eta_0^2} A_{\lambda\mu}(l_i) |I_{\lambda\mu}(\xi, \epsilon_0)|^2, \tag{22}$$
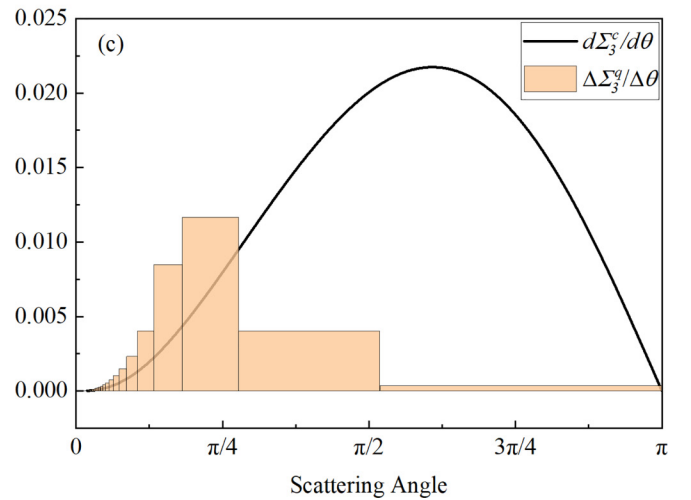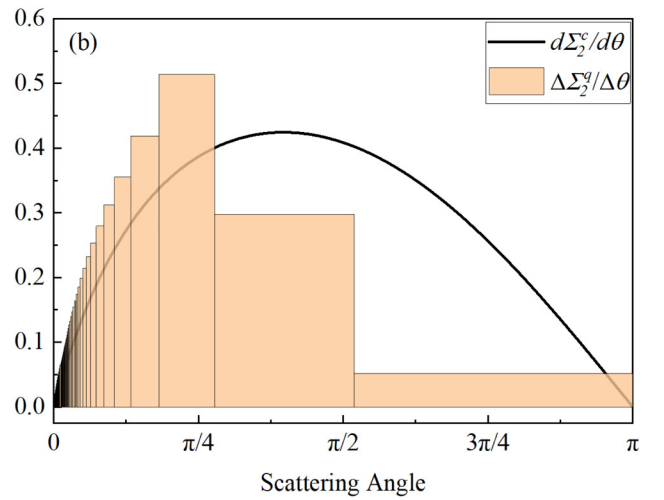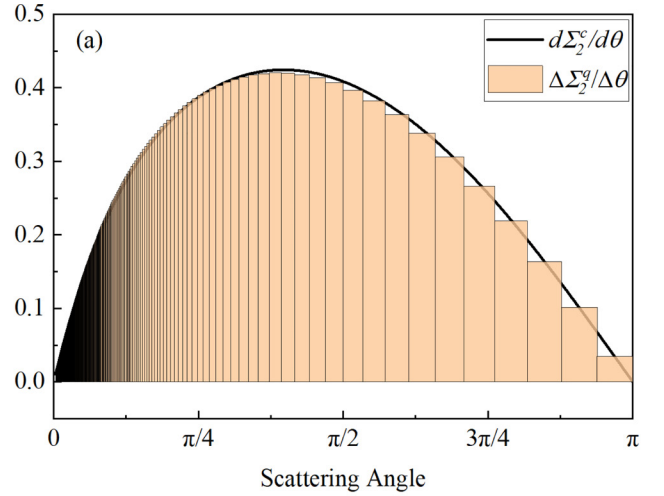

FIG. 5. The comparison between $d\Sigma_\lambda^c/d\theta$ from the SC method (solid line) and $\Delta\Sigma_\lambda^q/\Delta\theta$ from the QM method under WKB approximation (bar graph). All graphs are fixed at $\xi = 0$. (a) $E2$ transition with $1/\eta_0 = 0.1$. (b) $E2$ transition with $1/\eta_0 = 1.0$. (c) $E3$ transition with $1/\eta_0 = 1.0$.

where

$$A_{\lambda\mu}(l_i) = (2l_i + 1)(2l_i + 2\mu + 1)$$
$$\times \frac{(2l_i + \mu + \lambda)!!(2l_i + \mu - \lambda - 1)!!}{(2l_i + \mu - \lambda)!!(2l_i + \mu + \lambda + 1)!!}. \quad (23)$$

To compare the cross sections obtained from the WKB approximation and the SC approach, it is helpful to define a dimensionless quantity

$$\Sigma_\lambda = \frac{\sigma_\lambda}{\left(\frac{Z_1 e}{\hbar v_i}\right)^2 a^{-2\lambda + 2} B(E\lambda)}. \quad (24)$$

Σ_λ for the two approaches are expressed as follows:

$$\Sigma_\lambda^q = \frac{16\pi^3}{(2\lambda + 1)^3} \frac{k_i k_f}{k_0^2} \sum_\mu \left| Y_{\lambda\mu}\left(\frac{\pi}{2}, 0\right) \right|^2$$
$$\times \sum_{l_i} \frac{1}{\eta_0^2} A_{\lambda\mu}(l_i) |I_{\lambda\mu}(\xi, \epsilon_0)|^2,$$

$$\Sigma_\lambda^c = \frac{16\pi^3}{(2\lambda + 1)^3} \sum_\mu \left| Y_{\lambda\mu}\left(\frac{\pi}{2}, 0\right) \right|^2$$
$$\times \int_0^\pi \frac{\cot\left(\frac{\theta}{2}\right)}{\sin^2\left(\frac{\theta}{2}\right)} |I_{\lambda\mu}(\xi, \epsilon)|^2 d\theta. \quad (25)$$

The difference between the two results can be clearly seen. The angular momentum l_i is related to the deflection angle θ of the classical orbit by $\theta = 2\operatorname{arccot}(l_i/\eta_0)$. In the classical limit $\eta_0 \gg 1$ and $l_i \gg 1$, the following replacements can be made:

$$\sum_{l_i} \rightarrow \frac{\eta_0}{2} \int_0^\pi d\theta \sin^{-2}\left(\frac{\theta}{2}\right),$$

$$A_{\lambda\mu}(l_i) \rightarrow 2l_i = 2\eta_0 \cot\left(\frac{\theta}{2}\right), \quad (26)$$

$$\epsilon_0 \rightarrow \epsilon.$$

Departing from the classical limit, Σ_λ^q can deviate substantially from Σ_λ^c, except for a coefficient $k_i k_f / k_0^2$, which causes no influence when $\xi = 0$.

We depict the comparison in Fig. 5, with the solid curve representing $d\Sigma_\lambda^c/d\theta$ from the SC approach and the bar graph indicating $\Delta\Sigma_\lambda^q/\Delta\theta$ from the QM approach under WKB approximation. Figures 5(a) and 5(b) present the comparison for $E2$ transition with $1/\eta_0 = 0.1$ and 1.0, respectively. For $1/\eta_0 = 0.1$, which is closer to the classical limit, the two results agree closely to each other. For $1/\eta_0 = 1.0$, however, substantial discrepancies can be seen.

Figure 5(c) presents the comparison for $E3$ transition with $1/\eta_0 = 1.0$. Upon comparing Figs. 5(b) and 5(c), it is evident that the increase in the order of multipole transitions significantly influences the results. As the order of multipole transitions increases, the disparity between $\Delta\Sigma_\lambda^q/\Delta\theta$ and $d\Sigma_\lambda^c/d\theta$ remains basically unchanged at small angles θ, while at large angles $\Delta\Sigma_\lambda^q/\Delta\theta$ becomes significantly smaller than $d\Sigma_\lambda^c/d\theta$, resulting in a predominant discrepancy between Σ_λ^c and Σ_λ^q. For $E4$ or $E5$ transition, a disparity of 1 to 3 orders of magnitude will emerge.

IV. CONCLUSION

In this paper we re-examine the commonly used SC approach for nuclear Coulomb excitation. We emphasize that the validity of the SC approach is established only for $E2$ transitions. For higher-order nuclear transitions, the accuracy of the SC approach remains inadequately benchmarked. Our findings indicate that for these higher-order multipole transitions, the SC approach can deviate significantly—by orders of magnitude—from QM results. We analyze and elucidate the shortcomings of the SC approach through the use of the WKB approximation.

[1] E. Fermi, Über die theorie des stoßes zwischen atomen und elektrisch geladenen teilchen, Z. Phys. **29**, 315 (1924).

[2] E. J. Williams, Nature of the high energy particles of penetrating radiation and status of ionization and radiation formulae, Phys. Rev. **45**, 729 (1934).

[3] K. Alder, A. Bohr, T. Huus, B. Mottelson, and A. Winther, Study of nuclear structure by electromagnetic excitation with accelerated ions, Rev. Mod. Phys. **28**, 432 (1956).

[4] P. H. Stelson and F. K. McGowan, Coulomb excitation, Annu. Rev. Nucl. Sci. **13**, 163 (1963).

[5] T. Glasmacher, Intermediate-energy Coulomb excitation, Nucl. Phys. A **693**, 90 (2001).

[6] A. Görgen and W. Korten, Coulomb excitation studies of shape coexistence in atomic nuclei, J. Phys. G **43**, 024002 (2016).

[7] R. Sherr, C. W. Li, and R. F. Christy, Coulomb excitation of F^{19} by alpha particles, Phys. Rev. **96**, 1258 (1954).

[8] G. F. Pieper and N. P. Heydenburg, Coulomb excitation of iron-57, Phys. Rev. **107**, 1300 (1957).

[9] C. E. Bemis, F. K. McGowan, J. L. C. Ford, Jr., W. T. Milner, R. L. Robinson, P. H. Stelson, G. A. Leander, and C. W. Reich, Coulomb excitation of states in ^{229}Th, Phys. Scr. **38**, 657 (1988).

[10] A. N. F. Aleixo and C. A. Bertulani, Coulomb excitation in intermediate-energy collisions, Nucl. Phys. A **505**, 448 (1989).

[11] D. C. Radford *et al.*, Coulomb excitation of radioactive ^{132,134,136}Te beams and the low $B(E2)$ of ^{136}Te, Phys. Rev. Lett. **88**, 222501 (2002).

[12] F. Becker *et al.*, Coulomb excitation of ^{78}Kr, Nucl. Phys. A **770**, 107 (2006).

[13] S. A. Gillespie *et al.*, Coulomb excitation of ^{80,82}Kr and a change in structure approaching $N = Z = 40$, Phys. Rev. C **104**, 044313 (2021).

[14] P. Spagnoletti *et al.*, Coulomb excitation of ^{222}Rn, Phys. Rev. C **105**, 024323 (2022).

[15] R. Anne *et al.*, Projectile Coulomb excitation with fast radioactive beams, Z. Phys. A **352**, 397 (1995).

[16] C. A. Bertulani, A. E. Stuchbery, T. J. Mertzimekis, and A. D. Davies, Intermediate energy Coulomb excitation as a probe of nuclear structure at radioactive beam facilities, Phys. Rev. C **68**, 044609 (2003).

[17] S. Ilieva *et al.*, Coulomb excitation of neutron-rich Cd isotopes, Phys. Rev. C **89**, 014313 (2014).

[18] H. Geissel, G. Munzenberg, and K. Riisager, Secondary exotic nuclear beams, Annu. Rev. Nucl. Part. Sci. **45**, 163 (1995).

[19] T. Motobayashi *et al.*, Large deformation of the very neutron-rich nucleus ^{32}Mg from intermediate-energy Coulomb excitation, Phys. Lett. B **346**, 9 (1995).

[20] A. Görgen, Shapes and collectivity of exotic nuclei via low-energy Coulomb excitation, J. Phys. G **37**, 103101 (2010).

[21] L. C. Biedenharn, J. L. McHale, and R. M. Thaler, Quantum calculation of Coulomb excitation. I, Phys. Rev. **100**, 376 (1955).

[22] G. Breit and P. B. Daitch, Correspondence between semiclassical and quantum treatments of Coulomb excitation, Phys. Rev. **96**, 1447 (1954).

[23] F. D. Benedict, P. B. Daitch, and G. Breit, Semiclassical approximation to Coulomb excitation integrals, Phys. Rev. **101**, 171 (1956).

[24] M. Samuel and U. Smilansky, Coulomb excitation near the Coulomb barrier, Phys. Lett. B **28**, 318 (1968).

[25] J. M. Hansteen and O. P. Mosebekk, Atomic Coulomb excitation by heavy charged particles, Nucl. Phys. A **201**, 541 (1973).

[26] I. Bloch, M. H. Hull, A. A. Broyles, W. G. Bouricius, B. E. Freeman, and G. Breit, Methods of calculation of radial wave functions and new tables of Coulomb functions, Phys. Rev. **80**, 553 (1950).

[27] P. B. Daitch, J. P. Lazarus, M. H. Hull, F. D. Benedict, and G. Breit, Validity of semiclassical treatment of Coulomb excitation, Phys. Rev. **96**, 1449 (1954).

[28] J. P. Lazarus and S. Sack, Agreement of classical and quantum Coulomb excitation integrals, Phys. Rev. **100**, 370 (1955).

[29] L. C. Biedenharn and C. M. Class, Soluble problem in the theory of Coulomb excitation, Phys. Rev. **98**, 691 (1955).

[30] L. C. Biedenharn, M. Goldstein, J. L. McHale, and R. M. Thaler, Quantum calculation of Coulomb excitation. II. Quadrupole excitation: Numerical results, Phys. Rev. **101**, 662 (1956).

[31] F. Salvat and J. M. Fernández-Varea, RADIAL: A Fortran subroutine package for the solution of the radial Schrödinger and Dirac wave equations, Comput. Phys. Commun. **240**, 165 (2019).

[32] F. Ajzenberg-Selove, Energy levels of light nuclei $A = 18$–20, Nucl. Phys. A **475**, 1 (1987).

[33] M. Arenz and R. Vianden, ^{83m}Kr, a potentially powerful PAC probe, Hyperfine Interact **222**, 73 (2013).

[34] Nuclear Structure and Decay Databases (2023), https://www.nndc.bnl.gov/.

[35] K. Alder and A. Winther, Theory of Coulomb excitation, Phys. Rev. **96**, 237 (1954).

[36] G. Breit and P. B. Daitch, Redistribution of classical and quantum densities, Proc. Natl. Acad. Sci. USA **41**, 653 (1955).